A&A 650, A10 (2021)
https://doi.org/10.1051/0004-6361/202039296

Astronomy & Astrophysics

Parker Solar Probe: Ushering a new frontier in space exploration

Special issue

Wave-particle energy transfer directly observed in an ion cyclotron wave

D. Vech[1], M. M. Martinović[2], K. G. Klein[2], D. M. Malaspina[1], T. A. Bowen[3], J. L. Verniero[3], K. Paulson[4], T. Dudok de Wit[5], J. C. Kasper[6], J. Huang[6], M. L. Stevens[4], A. W. Case[4], K. Korreck[4], F. S. Mozer[3], K. A. Goodrich[3], S. D. Bale[3], P. L. Whittlesey[3], R. Livi[3], D. E. Larson[3], M. Pulupa[3], J. Bonnell[3], P. Harvey[3], K. Goetz[7], and R. MacDowall[8]

[1] Laboratory for Atmospheric and Space Physics, University of Colorado, Boulder, CO, USA
e-mail: daniel.vech@lasp.colorado.edu
[2] Lunar and Planetary Laboratory, University of Arizona, Tucson, AZ 85719, USA
[3] Space Science Laboratory, University of California Berkeley, Berkeley, CA, USA
[4] Smithsonian Astrophysical Observatory, Cambridge, MA 02138, USA
[5] LPC2E, CNRS and University of Orléans, Orléans, France
[6] Climate and Space Sciences and Engineering, University of Michigan, Ann Arbor, MI 48109, USA
[7] School of Physics and Astronomy, University of Minnesota, Minneapolis, MN, USA
[8] NASA Goddard Space Flight Center, Greenbelt, MD, USA

Received 30 August 2020 / Accepted 28 October 2020

ABSTRACT

Context. The first studies with Parker Solar Probe (PSP) data have made significant progress toward understanding of the fundamental properties of ion cyclotron waves in the inner heliosphere. The survey mode particle measurements of PSP, however, did not make it possible to measure the coupling between electromagnetic fields and particles on the time scale of the wave periods.
Aims. We present a novel approach to study wave-particle energy exchange with PSP.
Methods. We used the Flux Angle operation mode of the Solar Probe Cup in conjunction with the electric field measurements and present a case study when the Flux Angle mode measured the direct interaction of the proton velocity distribution with an ion cyclotron wave.
Results. Our results suggest that the energy transfer from fields to particles on the timescale of a cyclotron period is equal to approximately 3–6% of the electromagnetic energy flux. This rate is consistent with the hypothesis that the ion cyclotron wave was locally generated in the solar wind.

Key words. solar wind – waves – turbulence

1. Introduction

In weakly collisional plasmas, such as the solar wind, resonant interactions between electromagnetic fields and particle distributions can lead to the transfer of energy from fields to particles and vice versa. For large-scale Alfvénic fluctuations, this exchange is largely oscillatory and dominated by undamped transfer back and forth between fields and particles. Near ion kinetic scales, the wave energy is irreversibly transferred to particles through the secular transfer of energy (Howes et al. 2017), leading to the collisionless damping of turbulent fluctuations, which has been observed in situ (Chen et al. 2019). Determining what mechanisms mediate this secular energy transfer is fundamentally important when describing the dissipation of turbulent energy in the solar wind, solar corona, planetary magnetospheres and laboratory plasmas. Example wave modes that may play an important role in this secular energy transfer in the solar wind include whistler, kinetic Alfvén waves (KAW), as well as ion cyclotron waves (ICW).

Ion cyclotron waves are quasi-parallel (with respect to the local magnetic field $\boldsymbol{B}_0$), left-hand polarized, and have a frequency near the proton gyrofrequency. They can be driven by departures from local thermodynamic equilibrium, for instance large proton temperature anisotropies, $T_\perp/T_\parallel > 1$ with orientations defined with respect to $\boldsymbol{B}_0$ or field-aligned differential flows between core protons, secondary beam populations and α-particles (Gary et al. 1993, 2003; Bale et al. 2009; Bourouaine et al. 2013; Verscharen et al. 2013a,b, 2019; Wicks et al. 2016; Klein et al. 2018; Woodham et al. 2019).

Initial observations from NASA's Parker Solar Probe (PSP, Fox et al. 2016), which is the first mission to have measured the solar wind below 0.3 au, have revealed that ICWs are abundant in the inner heliosphere and are observed in 30–50% of intervals with radially-aligned magnetic fields (Bale et al. 2019; Bowen et al. 2020a,b; Verniero et al. 2020). The lack of strong scaling of wave amplitudes with radial distance suggests that the observed ICWs are locally driven by temperature anisotropies or relative drifts. The survey data from the Solar Probe Analyzer for Ions (SPAN-I, 0.14 Hz cadence) and Solar Probe Cup (SPC, 1.15 Hz cadence, Case et al. 2020) have made it possible to measure the statistical properties of proton velocity distributions during the ICW events. However, the survey data are not fast enough to measure the coupling between electromagnetic fields and proton distributions on a time scale of the wave periods, which is necessary to quantify secular energy exchange between fields and particles.

The Flux Angle operation Mode (FAM) of SPC measures the phase space density fluctuation in a relatively narrow range (≈15 km s^{-1} wide window) of the proton velocity distributions for short intervals (≈1 min intervals four times a day) with up to 293 Hz cadence. The speed range scanned by the FAM is adjustable and it can be set to measure any part (e.g. core, beam, tail) of the proton velocity distribution functions. FAM data were first used to study cross helicity and residual energy at kinetic scales (Vech et al. 2020). These initial results show that the noise floor of the FAM for turbulent amplitudes measured during PSP's first perihelion is approximately 7 Hz, which is higher than the typical ion-scale spectral break of 0.3–2 Hz (Duan et al. 2020). High cadence FAM data, in conjunction with the simultaneous measurements of the electric field (Bale et al. 2016), may allow for the measurement of secular energy transfer using a variation of the recently developed wave-particle correlation method of Howes et al. (2017), which we refer to as "the standard wave-particle correlation" technique throughout this paper. This technique was successfully applied to identify signatures of electron Landau damping in the turbulent terrestrial magnetosheath (Chen et al. 2019), but has it has not been applied to PSP data yet.

This paper presents new observations of wave-particle energy exchange involving an ICW, which was observed during the third PSP perihelion at 0.23 AU. We measured the transfer of energy from electromagnetic fields to particles with a variation of the wave-particle correlation technique described above. Our results suggest that the energy transfer from fields to particles on the timescale of a cyclotron period is equal to approximately 3–6% of the electromagnetic energy flux. This rate is consistent with the hypothesis that the ion cyclotron wave was locally generated in the solar wind.

2. Summary of the ICW event

An ICW event was observed by FIELDS on 28 Aug 2019 from 00:08:58-00:09:08. The SPC was operated in FAM with a 71.4 Hz cadence on 28 Aug 2019 between 00:08:46-00:09:51, measuring the entire wave event. Figure 1a shows the magnetic field components for this interval in the RTN system (R points radially outward from the Sun, N is along the ecliptic north and T completes the right-hand coordinate system) using the fluxgate magnetometer data with the 66 s average subtracted from each component. Figure 1b shows the trace power spectra of magnetic field fluctuations obtained with a continuous wavelet transform. Figures 1c and d show the results of the minimum variance analysis in the maximum-to-intermediate and maximum-to-minimum planes (Sonnerup & Cahill Jr 1967) for the interval marked with an arrow in Fig. 1a. The minimum variance direction ([0.93 −0.27 −0.23] in the RTN frame) is within 2° with respect to the background magnetic field ($|B_0|$ = 44.9 nT). The angle between R and the magnetic field direction (θ_{BR}) was 157°. The ratio of the maximum to intermediate eigenvalue is $\lambda_{max}/\lambda_{int}$ = 1.15 while the maximum to minimum eigenvalue is $\lambda_{max}/\lambda_{min}$ = 17.9; they are both consistent with a circularly polarized wave.

Figures 1e–g show the power spectra density of the electric field, the differential charge flux density, and the magnetic field using 66 s of data from the FAM interval. The differential charge flux density corresponds to the current density (in units of pA cm^{-2}) on the SPC collector plates due to solar wind protons. The wave activity between 1.4–2.3 Hz is seen as enhanced wave power in all three panels. In the frequency range of the wave activity, the amplitude of the differential charge flux fluctuations

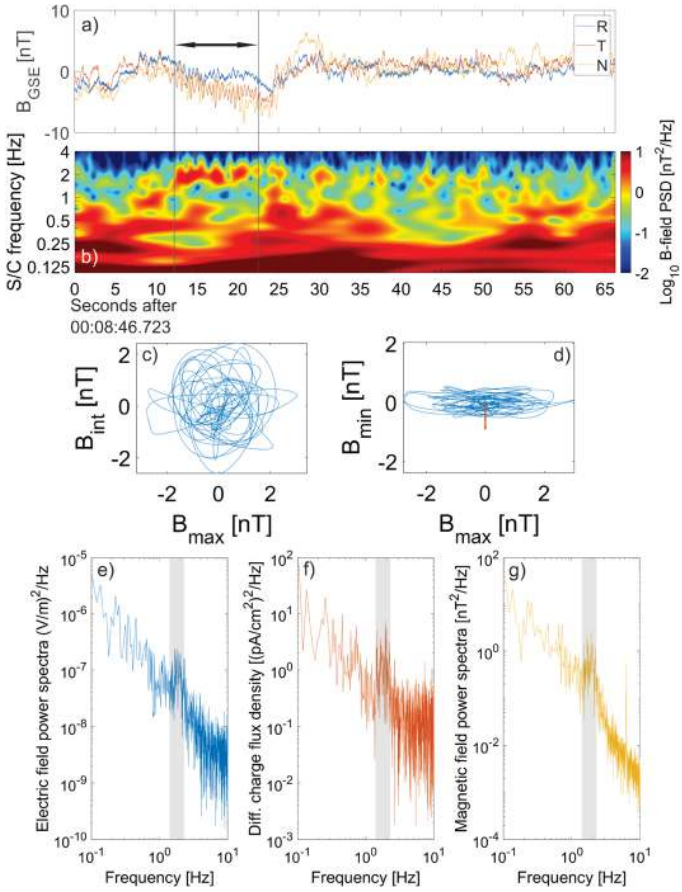

Fig. 1. (*a*) Fluxgate magnetometer data (66 s averaged subtracted) and (*b*) trace power spectra of the magnetic field fluctuations. (*c* and *d*) Hodograms showing band-pass filtered (0.6–4 Hz) fluctuations for the interval marked with an arrow in *panel a* in the maximum-intermediate and maximum-minimum variance planes. The red arrow in *panel d* shows B_0. *Panels e–g*: power spectra density of the electric field, differential charge flux density and magnetic field fluctuations, respectively. The frequency range with wave activity (1.4–2.3 Hz) is marked with gray shade.

is approximately one order of magnitude larger than at slightly lower (1 Hz) and higher (3 Hz) frequencies, respectively. It can also be seen that the noise floor of the FAM measurements (flattening spectra) is approximately 4 Hz. Based on these results, we suggest that the FAM measurements at the frequency of the wave are not affected by noise.

We used the approach of Vech et al. (2020) to calculate the RTN proton velocity fluctuations in the FAM interval and then transformed them into the minimum variance frame, which was determined previously from the magnetic field data. The phase speed of the wave was obtained with the technique of Bowen et al. (2020b) derived from Ohm's law and Faraday's law: $V_{ph}^2 = \delta V_\perp^2 B_\parallel^2 / \delta B_\perp^2$ where $B_\parallel$ is the minimum variance component of the magnetic field, and $\delta B_\perp$ and $\delta V_\perp$ are the amplitudes of the magnetic field and velocity fluctuations that are perpendicular with respect to $B_\parallel$. We find that the average and standard deviation of V_{ph}/V_A over the interval with the wave activity is 0.65 ± 0.12, which is consistent with an ion cyclotron wave (see Fig. 3 in Bowen et al. 2020b).

Figure 2 shows the proton velocity distributions (5 s averages) immediately before and after the FAM interval. The shaded area shows the range of speeds (257.2–278.2 km s^{-1} in the RTN

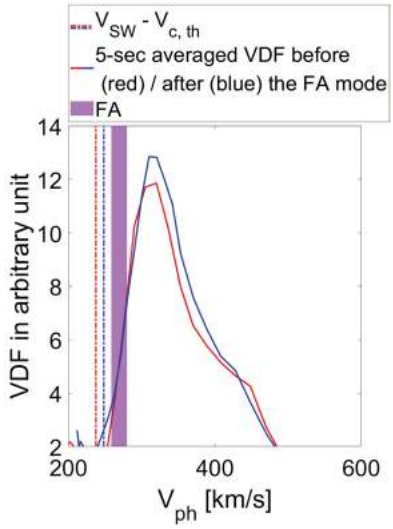

Fig. 2. 5-s averages of the proton velocity distributions before (red) and after (blue) the FAM interval. The range of phase speeds measured by the FAM are shaded. The proton core thermal speed (with respect to the core proton speed) is marked with a dashed line.

Table 1. 5-s averages and standard deviations of solar wind parameters before and after the FA mode interval.

Parameter	Before	After
V_c [km s^{-1}]	300 ± 5.3	316 ± 12.1
n_c [cm^{-3}]	150 ± 16.9	139 ± 19.4
$V_{c,th}$ [km s^{-1}]	79.5 ± 5.7	69.6 ± 5.9
V_b [km s^{-1}]	413 ± 5.3	428 ± 12.1
n_b [cm^{-3}]	17.8 ± 16.9	4.5 ± 19.4
$V_{b,th}$ [km s^{-1}]	52 ± 5.7	30.3 ± 5.9
V_A [km s^{-1}]	78.1 ± 5.1	83.1 ± 4.6
$T_\perp/T_\parallel$	1.78 ± 0.3	1.17 ± 0.25
$\beta_{p\parallel}$	0.64 ± 0.26	0.62 ± 0.22
$\beta_{p\perp}$	1.15 ± 0.24	0.73 ± 0.23
$\|B\|$ [nT]	44.9 ± 0.25	44.9 ± 0.48

Notes. The c and b subscripts correspond to the core and beam, respectively, and the p subscript corresponds to fits of the entire proton distribution. The ratio of the proton thermal pressure (defined with respect to the background magnetic field) to magnetic pressure are denoted with $\beta_{\parallel p}$ and $\beta_{\perp p}$.

frame) measured by the FA mode. As SPC measures only a single energy per charge window during a FAM, bulk solar wind parameters are not available.

Table 1 compares the core plasma parameters before and after the FAM interval. We find less than a 15% change in the core proton values, and that the flow angle was closely aligned (9.3°) with the normal of the SPC collector plate. These results suggest that SPC approximately measured the same part of the velocity distribution in the FAM and there were no significant fluctuations in the core parameters. The proton beam density and temperature showed larger variability, changing by a factor of 3.95 and 1.71, respectively. The proton temperature anisotropy ($T_\perp/T_\parallel$) was 1.78 and 1.17 before and after the FAM interval, respectively, which are consistent with an Alfvén-cyclotron instability. Proton temperature anisotropy measurements made with SPC were determined by examining the change in the

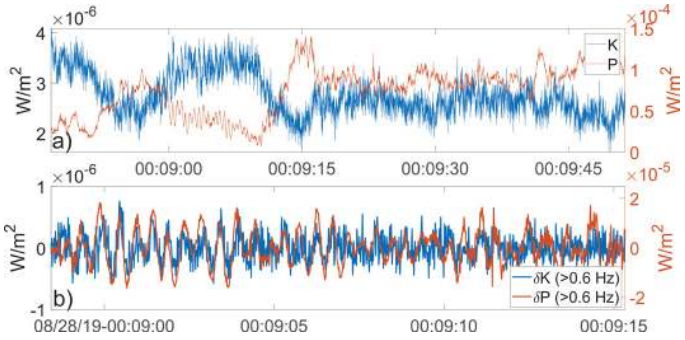

Fig. 3. (a) P and K for the entire studied interval, the magnitude of P is larger by a factor of 20–50 than K and (b) the high frequency (>0.6 Hz) fluctuations for the sub-interval with the wave activity.

apparent flow angle across the peak of the observed velocity distribution function. This measurement was made separately in the x–z and y–z planes in spacecraft coordinates, and the final value is a combination of the two, which are weighted by uncertainty and assuming gyrotropy. For details on this approach see Paulson et al. (in prep.).

3. Quantifying rate of energy transfer

The standard wave-particle correlation technique relies on three-dimensional velocity distributions and three-dimensional measurements of the electric field. However, SPC only measures the reduced velocity distribution in the plane of the collector plate. The FIELDS instrument measures only the radial electric field fluctuations for high frequencies (above the kilohertz range) and thus low frequency E-field is only available in the plane of the heat shield (e.g., T and N components). For an analysis of PSP data, and in particular for the velocity-range limited FAM observations, the wave-particle correlation technique needs to be modified to estimate the energy transfer between fields and particles.

First, we calculated the Poynting flux of the electromagnetic field by using the T and N components of the $\boldsymbol{E}$ and $\boldsymbol{B}$ fields

$$P = (0, E_T, E_N) \times (0, B_T, B_N)/\mu_0 [\mathrm{W\,m^{-2}}] \quad (1)$$

and the energy flux of the solar wind protons in the range of the FAM is

$$K = \frac{1}{2} \cdot m_p \cdot v_0^2 \cdot \phi_p [\mathrm{W\,m^{-2}}], \quad (2)$$

where ϕ_p is the proton flux [$\#/(m^2 \cdot s)$] measured by the FAM, $v_0 = -38.8$ km s^{-1} is the center of the FAM speed range with respect to the average core proton speed (see Fig. 2) and m_p is the mass of a proton.

Figure 3a shows the derived K and P parameters for the entire selected interval while Fig. 3b focuses on the subinterval with the ICW and shows the high pass filtered (at 0.6 Hz) P and K parameters, δP and δK. The remarkably strong correlation between δK and δP suggests that significant transfer of energy between the fields and particles may take place in the ICW. We note that measuring high correlation between fields and particles is necessary, but not sufficient condition for wave damping (see Gershman et al. 2017), and the secular energy transfer is tested with the following analysis.

To quantify the transfer of energy between the electric field and solar wind protons within the FAM energy range, we modified the approach of Howes et al. (2017) to the following expression

$$C_{\mathrm{FAM};\|,\perp} = q_p v_0 \delta E_{\|,\perp} \delta \phi_p \quad (3)$$

with the time-integrated value $\int C_{\mathrm{FAM}}(t)\mathrm{d}t$ representing the transfer of energy flux, in [W m^{-2}], mediated by protons with energies within the FAM range. In Eq. (3), q_p is the charge of a proton, and $E_\|$ and $E_\perp$ correspond to the electric field fluctuations parallel and perpendicular with respect to the magnetic field in the T-N plane. The direction of $E_\perp$ is defined by the cross product of the +R unit vector and the magnetic field in the T-N plane (0, B_T, B_N).

The proposed technique allowed us to identify whether the energy exchange is preferentially coupled to $E_\|$ or $E_\perp$. We note that in order to identify the secular energy transfer, both ϕ_p and $E_{\|,\perp}$ were high pass filtered at 0.6 Hz to remove any constant phase space density and electric field structures (hence the δ notation in Eq. (3)). A similar filtering technique was used by Chen et al. (2019) as well. For our analysis the electric field data measured in the spacecraft frame (E_sc) was converted into the frame of the solar wind: $\boldsymbol{E}_\mathrm{sw} = \boldsymbol{E}_\mathrm{sc} + \boldsymbol{v}_\mathrm{sw} \times \boldsymbol{B}$ (Chen et al. 2011). For the calculation of $\boldsymbol{v}_\mathrm{sw}$ during the FAM interval, we used the approach of Vech et al. (2020).

We calculated $\int C_{\mathrm{FAM}}(t)\mathrm{d}t$ for 3-s blocks of data. The length of this interval ensures that multiple (≈6) wave periods are included. In the absence of secular energy transfer $\int C_{\mathrm{FAM}}(t)\mathrm{d}t$ is zero over multiple wave periods since the oscillatory transfer of energy between fields and particles averages out. We adjusted the measured $\int C_{\mathrm{FAM}\|;\perp}\mathrm{d}t$ values by multiplying them with the ratio of the cyclotron period ($2\pi/\Omega_p$ = 1.46 s) and the length of the integration window (3-s); therefore, the computed values correspond to the average transfer of energy flux on the time scale of a cyclotron period.

We tested the statistical significance of the measured $\int C_{\mathrm{FAM}}(t)\mathrm{d}t$ with the phase-randomized technique suggested by Howes et al. (2017). The electric field data are Fourier transformed, a uniformly distributed random phase is added, and the data is inverse Fourier transformed. We calculated $\int C_{\mathrm{FAM}}(t)\mathrm{d}t$ 40 times for each 3-s block of data with the randomized electric field data and obtain a distribution of the possible values.

The results of the analysis are presented in Fig. 4. In panels a and c the gray and black bars correspond to the 1 and 2σ distributions of $\int C_{\mathrm{FAM}}(t)\mathrm{d}t$ calculated with randomized electric field data, respectively and the blue bars show the $\int C_{\mathrm{FAM}\|;\perp}\mathrm{d}t$ values calculated with the real electric field data. It can be seen that there is a 12-s interval where the $\int C_{\mathrm{FAM}\perp}\mathrm{d}t$ values are statistically significant on the 2σ level, which overlaps with the wave activity presented in Fig. 1a. The positive sign of $\int C_{FAM\|;\perp}\mathrm{d}t$ is consistent with the transfer of energy flux from electromagnetic fields to particles (Chen et al. 2019; Klein et al. 2016). For the same interval the $\int C_{\mathrm{FAM}\|}\mathrm{d}t$ values were statistically significant for only two 3-s segments of data. At around the 25th second both $\int C_{\mathrm{FAM}\|}\mathrm{d}t$ and $\int C_{\mathrm{FAM}\perp}\mathrm{d}t$ are statistically significant; however, this is likely caused by a magnetic discontinuity (see the change of the magnetic field components in Fig. 1a) and not by an ICW.

In order to understand the significance of the measured $\int C_{\mathrm{FAM}\|;\perp}\mathrm{d}t$ values during the wave event, we compared them to the average magnitude of the high pass filtered (at 0.6 Hz) P parameter ($|\delta P|$) in each 3-s bin. The ratio of $\int C_{\mathrm{FAM}\perp}\mathrm{d}t$ and $|\delta P|$

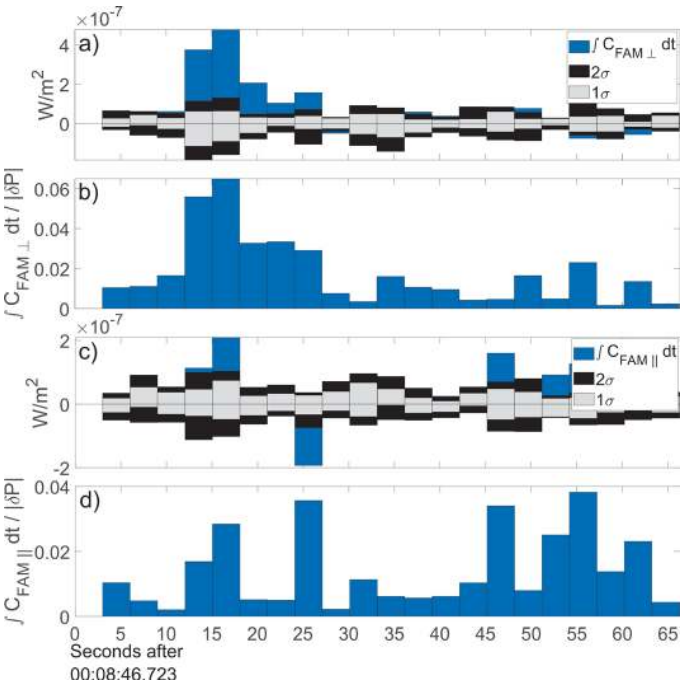

Fig. 4. (*a–c*) $\int C_{\mathrm{FAM}\|;\perp}\mathrm{d}t$. The gray and black bars show the 1 and 2σ values of $\int C\mathrm{d}t$ calculated with the synthetic (randomized) electric field data. (*b–d*) Ratio $\int C_{\mathrm{FAM}\|;\perp}\mathrm{d}t$ and the average of $|\delta P|$ fluctuations in each 3-s block of data.

suggests that the exchange of energy flux between $E_\perp$ and particles on the time scale of a cyclotron period is approximately 3–6% of the amplitude of Poynting flux fluctuations while it is approximately 3% for $E_\|$. These results correspond to $\gamma/\Omega_p \in [0.032; 0.066]$. Due to the limitation of the measurements (two-dimensional plane geometry), the derived damping rates should be considered as lower thresholds. However, we suggest that the bulk of the energy transfer is still captured since the largest amplitude electric field fluctuations are approximately in the T-N place and the largest amplitude particle flux fluctuations are in the R component.

The full equation of the Poynting theorem includes the following three terms: $\boldsymbol{j} \cdot \boldsymbol{E}$ (represented by $\int C_{\mathrm{FAM}}(t)\mathrm{d}t$), the Poynting flux term (represented by P) and $\partial/\partial t(\epsilon|E|^2 + |B|^2/\mu)$. We suggest that the latter term has a negligible amplitude compared to the Poynting term due to the fact that the ICW is a highly incompressible structure where fluctuations in the magnitude of the electromagnetic field are significantly smaller than the components perpendicular to the wave propagation. We tested this assumption for the magnetic field (where all three components are available) and find that $dB_\perp/\delta|B| \approx$ 50–200 at the wave frequency. The $\partial/\partial t(\epsilon|E|^2 + |B|^2/\mu)$ term also includes secular changes in the amplitude of E and B on quasilinear timescales related to γ/Ω_p. We find that the power spectra based on the T and N components of E and B fields has factor of ≈100 larger amplitude than the power spectra of |E| and |B| (both measured in the T-N plane). Therefore we quantify the field-particle energy transfer with Eq. (3) and the Poynting term.

4. Linear stability analysis of the ICW event

Using the PLUME numerical solver (Klein & Howes 2015) we calculated linear dispersion relations for the plasma parameters before the FAM. PLUME calculates the linear normal mode

response for an arbitrary number of relatively drifting, bi-Maxwellian ion and electron populations. We modeled the plasma with separate proton core and beam components and a single electron distribution, using the measurements from the "before" interval (see Fig. 2) to yield dimensionless parameters $\beta_{\parallel,c} = 0.947$, $V_{\parallel,c,th} = 2.265\times10^{-4}c$, $T_{\parallel,b} = 0.43T_{\parallel,c}$, $n_b = 0.11n_c$, and $T_{\parallel,e} = 1.00T_{\parallel,c}$. The value of $\beta_{\parallel,c}$ is based on the ratio of the thermal pressure associated with the core proton distribution (where the core and beam are Maxwellian fits to the SPC measurements of the proton velocity distribution) to the magnetic pressure, rather than the total proton thermal pressure extracted from an analysis of the moments ($\beta_{p\parallel}$ parameter listed in Fig. 2). The relative drift speed between the beam and core was set to $1.41V_A$.

Using the method described in Paulson et al. (in prep.), the total proton temperature anisotropy was found to be $T_{\perp,p}/T_{\parallel,p} = 1.79$. Given the uncertainties in this method, and in disentangling anisotropies in the core from the total anisotropy, we consider solutions with $T_{\perp,c}/T_{\parallel,c} = 1.0, 1.4$, and 1.8. The electrons and proton beam were assumed to have isotropic temperatures.

We identified both the forward and backward propagating Alfvén waves at $k_\perp\rho_c = k_\parallel\rho_c = 10^{-3}$ (where ρ_c is the proton gyroradii; $k_\perp$ and $k_\parallel$ are the parallel and perpendicular wavenumbers defined with respect to $\boldsymbol{B}_0$), and traced these normal mode solutions to larger $k_\parallel$ for fixed $k_\perp$. The backwards propagating solutions, with cyclotron resonant velocities greater than the core proton velocity are found to be stable for all three anisotropies considered. The characteristics of the forward solutions are shown in Fig. 5 where we make a direct comparison with the wave parameters (shaded areas in each panel) derived in the previous sections.

Figure 5a shows the Doppler shifted wave frequency as a function of $k_\parallel\rho_c$. The gray shade corresponds to the observed frequency of the wave (see Figs. 2e–g), which constrains the range of $k_\parallel\rho_c$ values to approximately $k_\parallel\rho_c \in [0.6; 1]$. In Figs. 5b and c, the computed V_{ph}/V_A ratio (see Sect. 2) and the empirically derived γ/Ω_p ratio (see Sect. 3) are consistent with the same range of $k_\parallel\rho_c$ values. In Fig. 5c the intersection of the shaded area with the line plots suggests that the wave undergoes damping for all three anisotropy values considered here.

In Fig. 5d, we calculated the resonant cyclotron velocities v_{res} as

$$v_{res} = \frac{\omega_r - n\Omega_p}{k_\parallel} \tag{4}$$

where ω_r is the real frequency, $n = +1$ for forward propagating Alfvénic solutions, as appropriate for their left-handed plasma frame polarizations. As the cyclotron resonant velocities for backward-propagating ICWs, with $n = -1$ due to their right-handed plasma-frame polarization (not shown), are at velocities greater than V_c, they are not resolved by this particular FAM observation. The velocity space observed by the FAM covers $v \in [-0.53; -0.27]V_A$ below V_c. Although the FAM range does not overlap with the v_{res}/V_A curves in the range of $k_\parallel\rho_c = [0.6; 1]$, the gap between them is only 13 km s^{-1} ($0.16V_A$) at $k_\parallel\rho_c = 1$.

Given the sign of the energy transfer measured by $\int C_{FAM\perp}dt$ and the comparison of the PLUME results with observations in Fig. 5, we suggest that our observations are consistent with an ICW being generated by a nearby region of plasma with a larger temperature anisotropy, which can then propagate to a region of lower anisotropy, where it can be efficiently absorbed. It is likely this last step that the FAM is observing.

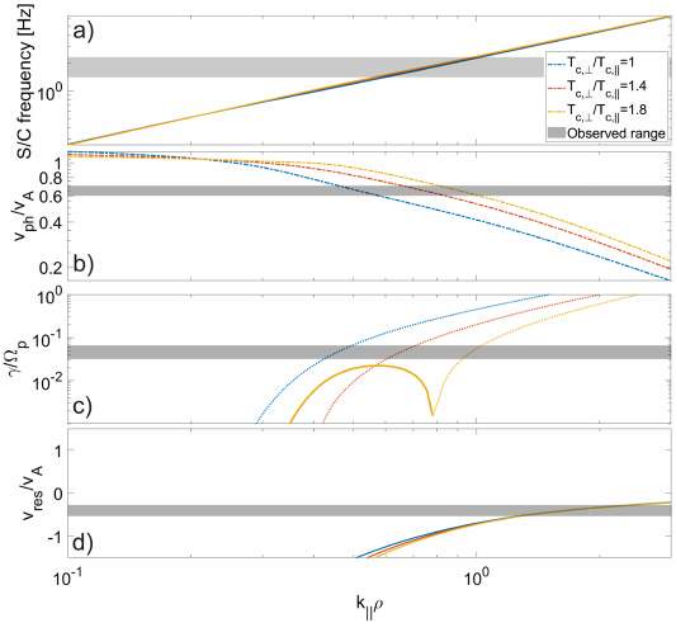

Fig. 5. Overview of the PLUME dispersion solution for forward propagating Alfvén/IC modes for varying $T_{\perp,c}/T_{\parallel,c}$. *Panel a*: Doppler shifted frequency, *panel b*: phase speed normalized by the Alfvén speed. *Panel c*: normalized growth (solid line) or damping (dashed) rate γ/Ω_p, which strongly depends on the temperature anisotropy. *Panel d*: ratio of the resonant velocity normalized by the Alfvén speed.

5. Conclusions

In this paper, we have described a method to measure the direction and magnitude of the energy flux transfer between electromagnetic fields and particles in the range of the Flux Angle mode of SPC. Measurements of the Doppler shifted wave frequency, phase speed and the γ/Ω_p damping ratio were in good agreement with the properties of an ICW with $k_\parallel\rho_c = [0.6; 1]$. Our results are consistent with the damping of an ICW where the energy flux is transferred from electromagnetic fields to the particles with a magnitude of approximately 3–6% (per cyclotron period) of the Poynting flux fluctuations.

The results make it possible to clarify where (local versus solar origin) the ICW was generated. At the time of the observation $\delta B/B_0 \approx 0.1$. If we assume that the decay rate of δB is in the range of 3 and 6% per cyclotron period and that $\delta B/B_0 < 1$ in an Alfvén wave, then the upper thresholds of the wave generation are 34.8 (50-s) and 71.6 (104-s) cyclotron periods before PSP observed the waves, respectively. These timescales are consistent with the hypothesis that the ICW was locally generated in the solar wind.

Acknowledgements. K.G.K. was supported by NASA Grant 80NSSC19K0912. The authors thank the Parker Solar Probe team, especially the FIELDS and SWEAP teams for their support. The FIELDS experiment on the Parker Solar Probe spacecraft was designed and developed under NASA contract NNN06AA01C. T.D. acknowledges support from CNES. All data used in this work are available on the FIELDS data archive: http://fields.ssl.berkeley.edu/data/ and the SWEAP data archive: http://sweap.cfa.harvard.edu/pub/data/sci/sweap

References

Bale, S., Kasper, J., Howes, G., et al. 2009, Phys. Rev. Lett., 103, 211101
Bale, S., Goetz, K., Harvey, P., et al. 2016, Space Sci. Rev., 204, 49
Bale, S., Badman, S., Bonnell, J., et al. 2019, Nature, 576, 237
Bourouaine, S., Verscharen, D., Chandran, B. D., Maruca, B. A., & Kasper, J. C. 2013, ApJ, 777, L3
Bowen, T. A., Mallet, A., Huang, J., et al. 2020a, ApJS, 246, 66
Bowen, T. A., Bale, S. D., Bonnell, J., et al. 2020b, ApJ, 899, 74
Case, A. W., Kasper, J. C., Stevens, M. L., et al. 2020, ApJS, 246, 43
Chen, C., Bale, S., Salem, C., & Mozer, F. 2011, ApJ, 737, L41
Chen, C., Klein, K., & Howes, G. G. 2019, Nat. Commun., 10, 1
Duan, D., Bowen, T. A., Chen, C. H., et al. 2020, ApJS, 246, 55
Fox, N., Velli, M., Bale, S., et al. 2016, Space Sci. Rev., 204, 7
Gary, S. P., Fuselier, S. A., & Anderson, B. J. 1993, J. Geophys. Res. Space Phys., 98, 1481
Gary, S. P., Yin, L., Winske, D., et al. 2003, J. Geophys. Res. Space Phys., 108, 1068
Gershman, D. J., Adolfo, F., Dorelli, J. C., et al. 2017, Nat. Commun., 8, 1
Howes, G. G., Klein, K. G., & Li, T. C. 2017, J. Plasma Phys., 83, 535830401
Huang, J., Kasper, Vech, J. C., Klein, D. K. G., et al. 2020, ApJS, 246, 70
Klein, K. G., & Howes, G. G. 2015, Phys. Plasmas, 22, 032903
Klein, K. G., Howes, G. G., TenBarge, J. M., & Valentini, F. 2016, J. Plasma Phys., 86, 905860402
Klein, K., Alterman, B., Stevens, M., Vech, D., & Kasper, J. 2018, Phys. Rev. Lett., 120, 205102
Sonnerup, B. Ö., & Cahill Jr, L., 1967, J. Geophys. Res., 72, 171
Vech, D., Kasper, J. C., Klein, K. G., et al. 2020, ApJS, 246, 52
Verniero, J., Larson, D., Livi, R., et al. 2020, ApJS, 248, 5
Verscharen, D., Bourouaine, S., & Chandran, B. D. 2013a, ApJ, 773, 163
Verscharen, D., Bourouaine, S., Chandran, B. D., & Maruca, B. A. 2013b, ApJ, 773, 8
Verscharen, D., Klein, K. G., & Maruca, B. A. 2019, Liv. Rev. Sol. Phys., 16, 5
Wicks, R., Alexander, R., Stevens, M., et al. 2016, ApJ, 819, 6
Woodham, L. D., Wicks, R. T., Verscharen, D., et al. 2019, ApJ, 884, L53